FILLER NETWORKING OF A NANOGRAPHITE WITH A HIGH SHAPE ANISOTROPY AND SYNERGISM WITH CARBON BLACK IN POLY(1,4-*CIS*-ISOPRENE)–BASED NANOCOMPOSITES

MAURIZIO GALIMBERTI,[1,2,*] VINEET KUMAR,[3] MICHELE COOMBS,[4] VALERIA CIPOLLETTI,[1] SILVIA AGNELLI,[5] STEFANO PANDINI,[5] LUCIA CONZATTI[6]

[1]POLITECNICO DI MILANO, DEPARTMENT OF CHEMISTRY, MATERIALS AND CHEMICAL ENGINEERING G. NATTA, VIA MANCINELLI 7, 20131 MILANO, ITALY
[2]CONSIGLIO NAZIONALE DELLE RICERCHE, ISMAC, VIA E. BASSINI 15, 20133, MILANO, ITALY
[3]UNIVERSITÀ DEGLI STUDI MILANO-BICOCCA, VIA R. COZZI 53, 20125 MILANO, ITALY
[4]PIRELLI TYRE, VIALE SARCA 222, 20126 MILANO, ITALY
[5]UNIVERSITÀ DEGLI STUDI DI BRESCIA, DIPARTIMENTO DI INGEGNERIA MECCANICA E INDUSTRIALE, VIA BRANZE 38, 25123 BRESCIA, ITALY
[6]CONSIGLIO NAZIONALE DELLE RICERCHE, ISTITUTO PER LO STUDIO DELLE MACROMOLECOLE, VIA DE MARINI 6, 16149 GENOVA, ITALY

RUBBER CHEMISTRY AND TECHNOLOGY, Vol. 87, No. 2, pp. 197–218 (2014)

ABSTRACT

A nanoGraphite (nanoG) having a high surface area and a high shape anisotropy, defined as the ratio between the crystallite dimensions in a direction orthogonal and parallel to structural layers, was used to prepare nanocomposites based on poly(1,4-*cis*-isoprene) (IR), in the neat polymer matrix and in the presence of carbon black (CB). Tensile and dynamic-mechanical measurements showed that nanoG forms a filler network at a relatively low concentration in neat IR and a hybrid filler network at a lower nanoG concentration in the presence of CB. A synergistic effect between the two carbon allotropes was found: composites containing both fillers present initial modulus values much higher than those calculated through the simple addition of the initial moduli of the composites containing only CB or nanoG. [doi:10.5254/rct.13.87903]

INTRODUCTION

The polymer world has been characterized, over the past years, by the appearance of the so-called nanofillers.[1,2] They are made by primary particles, with at least one dimension of one or few nanometers, that can be individually dispersed in the polymer matrix. Conversely, traditional fillers such as carbon black (CB) and silica are nanostructured: they are made by particles aggregates that cannot be separated through a thermomechanical mixing.[3] Most investigated nanofillers are organically modified clays (OC)[1,2,4–6] and carbon nanotubes (CNTs).[1,2,7] They have features of great importance for the reinforcement of polymer matrices: a large specific surface area and a high length-to-width ratio, which is a high aspect ratio. Thanks to these features, both OC (Refs. 8–10) and CNT (Ref. 11) require low content (less than 10% by weight) in a polymer matrix to form filler networks, provided that they are mostly dispersed as single or few layers or tubes. As a consequence, with very low nanofiller content, is possible to obtain high values of Young modulus for a thermoplastic matrix and a remarkable effect on the viscoelastic properties for polymer melts and elastomers.

Nowadays, the research is mainly focused on carbon nanofillers. Besides CNT, a steadily increasing interest is for graphene, a two-dimensional (2D) sheet made of sp^2-hybridized carbon atoms in an extended honeycomb network.[12] At the origin of said interest are its excellent thermal, electrical, and mechanical properties and its layered structure. Graphene has been demonstrated as the thinnest material on earth,[13] thus presenting a very high aspect ratio. The theoretical elastic modulus of a graphene sheet is greater than 1 TPa, and the Young modulus is about 1060 MPa,

*Corresponding author. Email: maurizio.galimberti@polimi.it

which is several times higher than that of a clay.[14,15] Remarkable efforts are thus made to prepare graphene or graphitic nanofillers made by few layers of graphene. These nanofillers are mainly called graphite nanoplatelets (GNP) but can also be called graphite nanosheets, graphite nanoflakes, or just simply exfoliated or expanded graphite (EG). Comprehensive reviews are already available on different types of graphite nanoparticles, reporting on their synthesis and modification[16,17] and processing.[18] In a recent review,[19] GNP are defined as a type of graphitic nanofillers composed of stacked 2D graphene sheets. GNP are characterized by a high surface area (theoretical value up to 2630–2965 m^2/g)[20] and by a high aspect ratio, when GNP aggregates are formed by a low number of sheets. In the literature, the reduction in the number of stacked layers in GNP is attempted through a variety of techniques, namely, intercalation, oxidization, heat treatment, microwave irradiation, and ultrasonic treatment.[21–24] A wide range of applications is envisaged for GNP, from sensors[25] and electromechanical resonators[26] to adsorbents.[27–29] GNP deserve increasing interest also as filler for polymers,[30] and reviews are already available on processing[18] and mechanical and electrical properties[31] of the ensuing polymer nanocomposites. GNP are used for thermoplastics, such as poly(ethylene) (PE),[32] ultra-high-molecular-weight PE,[33] poly(propylene),[34–37] poly(styrene),[38,39] poly(ethyleneterephtalate),[40] poly(methylmethacrylate),[41,42] poly(urethane),[43] poly(-carbonate),[44] poly(vinylidenefluoride),[45] poly(etherimide),[46] and poly(lactide),[47] and for thermosets, such as epoxy resins.[48] Improvements of mechanical, electrical, thermal, and oxygen barrier properties are reported.

In the case of elastomers, papers are available for natural rubber (NR),[49–55] poly(styrene-co-butadiene) (SBR),[55–58] poly(butadiene-co-acrylonitrile) (NBR),[55,59–62] carboxylated NBR,[63] fluoroelastomers,[64] and silicon rubber.[65] GNP led to the improvement in the following properties: mechanical,[49–61,63] electrical,[51–55,57,58,62–64] thermal,[51–53,55,57,58,63,65] barrier,[55] tribological,[57–60,63] wear resistance,[55] and friction coefficient.[61] GNP were used in their pristine state or underwent various treatments in order to achieve a higher level of exfoliation. For example, pristine GNP having a thickness of 10 nm were used to prepare electrically conductive NBR-based composites,[62] finding 0.5 phr as the percolation concentration and a high sensitivity to compression strain in the region of the percolation transition. EG was obtained by microwave irradiation of graphite oxide and was subsequently suspended in an aqueous medium as graphite nanosheets with the help of a surfactant and microwave irradiation.[60] Nanocomposites were finally prepared by adding, under vigorous stirring, NBR latex. The presence of these graphite nanosheets in nanocomposites containing also a large amount of CB led to enhanced tensile and dynamic mechanical properties and to a reduced coefficient of friction and specific wear rate. Moreover, the presence of EG incremented the tensile strength of SBR-based nanocomposites.[56] To introduce more acid and hydroxyl groups onto the graphene layers, commercially available EG was oxidized with acids.[53] From solution blending, a master batch based on said modified EG and epoxidized NR was then prepared and finally mixed with NR through melt blending. Improved mechanical, thermal, and dynamic-mechanical properties were obtained. An exfoliated graphite was synthesized by the acid intercalation method[64] and used for the preparation of nanocomposites based on a fluoroelastomer with 71 wt% as the fluorine content. The filler–polymer interaction and interaggregate interactions were hypothesized by observing the decrease in the intensity of the tanδ curve from dynamic-mechanical analysis. The formation of an interphase layer between the filler and the polymer matrix was also proposed on the basis of the rapid decrease of storage modulus on increasing the strain amplitude.

The main objective of the present work was to obtain graphite/elastomer nanocomposites characterized by continuous filler networks formed at low nanofiller content without any treatment of the pristine graphite. A key step was thus the selection of the appropriate pristine graphite grade, indicated in this work as nanoG, to be distinguished from the GNP samples reported in the literature. NanoG has a high surface area and high shape anisotropy,[66] defined as the ratio between the crystallite dimensions in directions orthogonal and parallel to structural layers. An accurate X-ray

diffraction (XRD) analysis recently demonstrated the high shape anisotropy of nanoG: this nanofiller is characterized by a low number of stacked graphene layers and by an extended crystalline order inside the structural layers.[66] On the basis of these structural features, the formation of filler networks at low nanoG content and a remarkable mechanical reinforcement should be expected.

For achieving an even nanoG distribution, poly(1,4-*cis*-isoprene) (IR) was selected as polymer matrix, with the aim of taking advantage of its characteristic strain-induced crystallization[67–72] and of the consequent high shear stress promoted during mixing. Said even distribution should be expected also on the basis of the Zeta potential (ZP) values of nanoparticles.[73–76] It is known that, in a dispersion, ZP is a measure of the repulsion between particles similarly charged. The dispersion becomes more stable and resistant to aggregation as ZP increases, and a good stability is achieved for ZP values from ± 40 mV.[77] The ZPs of graphite and graphene dispersions were measured and found to indicate stable dispersions at pH ≥ 7,[74,78] reaching a maximum at 9–10 as pH range.[75,76] Rubber compounds, which are slightly alkaline, could thus be an ideal environment to prevent graphite nanoparticle aggregation. Moreover, it is acknowledged that ZP can be applied not only to aqueous dispersions but also to viscous fluids, such as polymer melts.[79–81]

IR-based composites containing from 1 to 60 parts per hundred rubber (phr) of nanoG were prepared by melt blending. Similarly, to explore synergisms between two carbon allotropes, composites with a hybrid filler system made by nanoG (from 1 to 12 phr) and CB (60 phr) were also obtained. The shape anisotropy of nanoG was assessed both in the pristine state and in the composites, by means of XRD analysis. NanoG dispersion in the IR matrix was studied through transmission electron microscopy (TEM). Quasi-static and dynamic-mechanical measurements were taken on cross-linked samples of both composite series. The initial elastic modulus, E, and the ultimate properties were obtained from stress–strain curves, determining E as the slope at the origin of the curves. Strain–sweep tests, carried out by applying to the composites cyclic deformations in the torsion mode, brought to determine both storage G' and loss G'' moduli. The dependence of both E and G' measured at minimum deformation ($G'\gamma_{min}$) on the nanoG content was studied to investigate the existence of a percolation threshold for the nanofiller in the IR matrix. The nonlinear behavior at a low amplitude of viscoelatic moduli was also examined. For the first time, the filler networking phenomenon, in neat hydrocarbon polymer matrix and in the presence of CB, was investigated for a nanographite with a high surface area and a high shape anisotropy, in its pristine state.

EXPERIMENTAL

MATERIALS

Synthetic poly(1,4-*cis*-isoprene) (IR) was from Nizhnekamskneftekhim Export (Nizhnekamsk, Russian Federation) with trade name SKI3 and 70 Mooney units as Mooney viscosity ($M_L(1+4)100$ °C).

NanoGraphite (nanoG) was Synthetic Graphite 8427® from Asbury Graphite Mills Inc. (Asbury, NJ, USA). Elemental analysis was performed, and the results, expressed as wt%, are carbon 99.5, hydrogen 0.4, nitrogen 0.1, and oxygen 0.0. Thus, the value of carbon content reported in the technical data sheet (at least 99 wt%) was substantially confirmed. The surface area was measured to be 330 m^2/g.

Carbon black N326 (CB), with 30 nm as the mean diameter of spherical primary particles, hexadecyltrimethylammonium bromide (CTAB) surface area of 85 m^2/g, iodine adsorption of 84 g/kg, and dibutylphthalate (DBP) adsorption number 72 mL/100 g, was obtained from Cabot (Boston, MA, USA). It was used as received.

TABLE I
FORMULATIONS OF COMPOSITES CONTAINING NANOG AS THE ONLY FILLER[a]

	Composite									
Nano G	G-0	G-1	G-2	G-4	G-8	G-12	G-16	G-20	G-40	G-60
phr	0	1	2	4	8	12	16	20	40	60
Volume fraction	0	0.0043	0.0086	0.0171	0.0337	0.0497	0.0652	0.0808	0.1495	0.2097

[a] Amount of ingredients is indicated in phr (parts per hundred polymer). IR = 100 phr. Further ingredients: ZnO 4, stearic acid 2, sulphur 2, CBS 1.

Ingredients for composite preparation were used as received: bis(3-triethoxysylilpropyl)tetrasulfide, Si69 (Degussa, Hanau, Germany), ZnO (Zincol Ossidi, Milano, Italy), stearic acid (Sogis, Cremona, Italy), N-(1,3-dimethylbutyl)-N-phenyl-p-phenylenediamine (6-PPD; Crompton, Middlebury, CT, USA), sulphur (Solfotecnica, Ravenna, Italy), phtalic anhydride (Aldrich, St. Louis, MO, USA), N,N-dicyclohexylbenzothiazol-2-sulfenamide (DCBS; Flexsys, Kingsport, TN, USA), and cyclohexylthiopthalimide (prevulcanization inhibitor; Santogard PVI, Flexsys).

PREPARATION OF COMPOSITES BY MELT BLENDING

Composites' preparation was performed following the same procedure already adopted in previous works of nanocomposites, based on clays[8] and CNT.[11]

Composites without CB. — A Brabender® type internal mixer, with a 50 mL mixing chamber, was used for the preparation of composites without CB. A standard procedure was adopted. IR was introduced into the mixer at 80 °C and masticated for 1 min. The nanoG was added, and mixing was carried out for 5 min. The master batch was discharged at a temperature between 110 and 115 °C. After 16 h, it was fed again into the mixer and mixed at 60 °C and 30 rpm for 1 min. ZnO and stearic acid were then added, performing the mixing for a further 2 min; sulphur and sulphenamide were finally added, discharging the compound after 2 min at about 60 °C. Composites were finally homogenized by passing them five times on a two-roll mill operating at 50 °C, with the front roll rotating at 30 rpm and the back roll rotating at 38 rpm, and 1 cm as the nip between the rolls. Composite formulations are shown in Table I.

Composites with CB. — Composites containing both CB and nanoG were prepared in two steps, following the procedure already reported for IR-based nanocomposites with CB/OC (Ref. 8) or CB/CNT (Ref. 11) as hybrid filler system. An IR/CB master batch was first prepared in a Banbury-type internal mixer with a 1050 mL mixing chamber. IR was introduced at 40 °C and masticated for 30 s with rotors rotating at 75 rpm. CB was then added, and mixing was carried out for 120 s. The master batch was discharged at approximately 140 °C after 3 min of mixing. This master batch was then used for the preparation of all the composites containing CB, adding various amounts of nanoG. The master batch was introduced into the Brabender-type internal mixer at 80 °C and masticated at 30 rpm for 60 s. Different amounts of nanoG were added following the procedure described above for composites without CB. Formulations of composites with CB are reported in Table II.

Cross-linking of Composites. — Cross-linking reactions were promoted, for all the prepared composites, by a typical sulphur-based curing system, made of activators (ZnO, stearic acid), sulphur, and an accelerator (CBS). The amount of ingredients is indicated in Table I and Table II for composites without CB and with CB, respectively. Cross-linking reactions were monitored through rheometric analysis carried out with a Monsanto moving die rheometer, performing tests at 151 °C,

TABLE II
FORMULATIONS OF COMPOSITES CONTAINING 60 PHR OF CB AND VARIOUS AMOUNTS OF NANOG[a]

	Composite						
Nano G	CB/G-0	CB/G-1	CB/G-2	CB/G-4	CB/G-6	CB/G-8	CB/G-12
phr	0	1	2	4	6	8	12
Volume fraction	0	0.0038	0.0075	0.0149	0.0222	0.0293	0.0434

[a] Amount of ingredients is indicated in phr (parts per hundred polymer). IR = 100 phr, CB = 60 phr. Further ingredients: ZnO 4, stearic acid 2, sulphur 2, CBS 1.

for 30 min, at an oscillation frequency of 1.67 Hz (100 oscillations per minute) and oscillation amplitude of ±0.5°. The following parameters are discussed in the following sections: t_{s1}, t_{90}, and M_H. t_{s1} is the time needed to have a torque equal to (M_L+1), t_{90} is the time of vulcanization required to have a torque value equal to $M_L+(90/100)(M_H-M_L)$, M_H is the maximum torque measured, and M_L is the minimum torque measured.

CHARACTERIZATIONS

Density measurements were performed according to standard method ISO 2781, by determining the weights of cross-linked composites in a fluid having a lower density (i.e., air and water). These measurements were carried out to control the correspondence of the experimental values with the theoretical ones expected on the basis of the composite formulation.

TEM analysis was performed with a Zeiss EM 900 microscope applying an accelerating voltage of 80 kV. Ultra-thin sections (about 50 nm thick) of cross-linked composites were prepared with a Leica EM FCS cryo-ultramicrotome equipped with a diamond knife by keeping the samples at −130 °C.

Wide-angle X-ray diffraction (WAXD) patterns were obtained, at 35 KV and 40 mA, with nickel-filtered Cu-Kα radiation (1.5418 Å), with an automatic Bruker D8 Advance diffractometer, in reflection. The intensities of the reflections in WAXD patterns reported in pictures in this article were not corrected for polarization and Lorentz factors, to allow a better visibility of the (00ℓ) peaks. *d*-spacings were calculated using Bragg's law. The $D_{hk\ell}$ correlation length of nanoG crystals was determined by applying the Scherrer equation:

$$D_{hk\ell} = K\lambda/(\beta_{hk\ell} \cos \theta_{hk\ell}) \quad (1)$$

where K is the Scherrer constant, λ is the wavelength of the irradiating beam (1.5419 Å, CuKα), $\beta_{hk\ell}$ is the width at half height, and $\theta_{hk\ell}$ is the diffraction angle. The introduction of a correction factor has to be used in case $\beta_{hk\ell}$ is lower than 1°.

Tensile tests were performed on cross-linked specimens, obtained from the IR composites, adopting the following procedure. Composites were passed through a two-roll mill for 10 times at 40 °C, and disks, with a diameter of 56 mm and thickness of 2 mm, were prepared upon vulcanizing for 20 min at 170 °C with 150 bar pressure. Dumbbell specimens according to type 2 of ISO 37:2011 were cut from the disks, having nominal gauge length dimensions of $2 \times 4 \times 20$ mm^3. For each material, tensile tests were carried out at room temperature by an Instron dynamometer (model 3366). Two series of experiments were performed on each material. The first series was performed to evaluate the initial elastic modulus, selecting 10 mm/min as the cross-head rate and setting the distance between grips equal to the gauge length (20 mm). The second series was carried out to evaluate the ultimate properties, using a cross-head rate of 100 mm/min and setting the distance between the grips larger than the gauge length. Cross-head rates lower than the standard 500 mm/

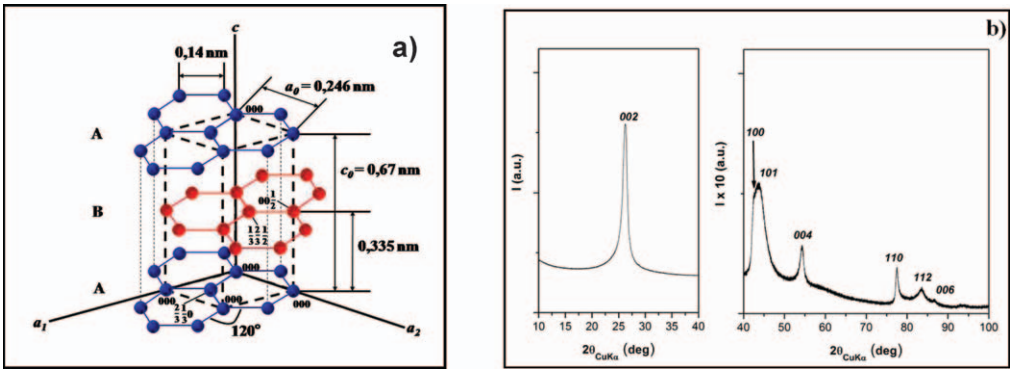

FIG. 1. — Crystalline structure of graphite (a) and X-ray diffraction (CuKα) pattern in the 2θ range of 5 to 80° of nanoG (b).

min were thus adopted. The 10 mm/min rate allowed an increase in data resolution and thus the accuracy for the determination of the initial elastic modulus at small strains. The higher 100 mm/min rate, chosen for the tests up to break, allowed a reduction in the overall time of the tests. Although mechanical properties of polymeric materials are rate dependent, the elastic modulus of rubbers in the plateau region has a negligible dependence on cross-head rate. The slope at the origin of the nominal stress–nominal strain curves was taken as the initial elastic modulus, *E*. Such a slope was obtained by fitting with a least-square regression line the data points at nominal strains smaller than 0.15%, where a linear stress–strain behavior is observed.

Dynamic-mechanical measurements in the torsion mode were carried out with a Monsanto R.P.A. 2000 rheometer. A first strain sweep (0.1–25% strain amplitude) was performed at 50 °C on un-cross-linked samples, to cancel their thermomechanical history. The samples were then kept in the instrument at the minimum strain amplitude (0.1%) for 1000 s to achieve fully equilibrated conditions. A strain sweep (0.1–25% strain amplitude) was then performed with a frequency of 1 Hz. Curing was carried out at 151 °C with a frequency of 1.67 Hz and an angle of 6.98%. Curing time for composites with or without CB was 20 or 30 min, respectively.

On cross-linked samples, a first strain sweep (0.1–25% strain amplitude) was performed at 50 °C, then the sample was kept in the instrument at the minimum strain amplitude (0.1%) for 1000 s, to achieve fully equilibrated conditions. Finally a strain sweep (0.1–25% strain amplitude) was performed with a frequency of 1 Hz. Values of G' at minimum deformation (0.28% strain), G' *(*γ *min)*, were taken upon achieving the fully equilibrated conditions.

RESULTS AND DISCUSSION

NANOG CHARACTERIZATION

The crystalline order of the high surface area graphite was studied by means of XRD analysis. Figure 1 reports the crystalline structure of graphite (Figure 1a) and the XRD pattern of the commercial sample of nanoG used in this work (Figure 1b). The XRD pattern of nanoG shows the following (00ℓ) reflections: (002) at 26.24° as 2θ value, corresponding to a d_{002} distance of 0.339 nm and (004) at 54.3° as the 2θ value. Figure 1a shows that, in the case of graphite, the d_{002} distance corresponds to the distance between A and B planes. The presence of the 100 and 110 reflections in XRD pattern at 42.7° and at 77.4°, as 2θ values, respectively, indicates a crystalline order in the structural layer.

As mentioned in the "Introduction" section, the dimension of graphite crystallites in the orthogonal and parallel directions with respect to structural layers was estimated from XRD data, by

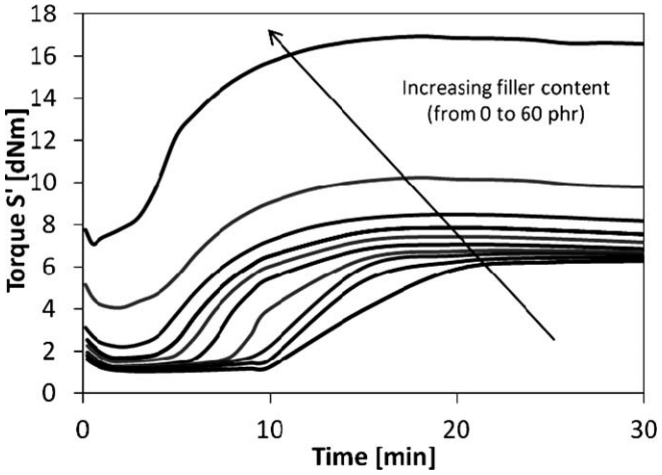

FIG. 2. — Cross-linking curves for IR-based composites with nanoG content from 0 to 60 phr (see Table I for formulations).

calculating the correlation length $D_{00\ell}$, which means the out-of-plane correlation lengths ($D_{\perp}$), and the correlation length D_{hk0}, which means the in-plane correlation length ($D_{\parallel}$). In particular, $D_{00\ell}$ was calculated by using the 002, 004, and 112 reflections, applying the Williamson and Hall plot[66,82]: a value of 9.8 nm was calculated. Taking into account that the d_{002} interlayer distance is 0.339 nm, a number of about 29 layers, stacked in an ordered manner, could be estimated. The in-plane correlation length ($D_{\parallel}$) was determined from the 100 and 110 reflections, finding a value of 30.2 nm. The shape anisotropy was calculated through the ratio $D_{\parallel}/D_{\perp}$, and a value of 3.1 was found. In a previous work,[66] nanoG was compared with several graphite grades, mainly thermally expanded graphites and calcinated petroleum coke. Shape anisotropy for these grades was in a range from 1 to 2.2. NanoG was thus found to have the highest shape anisotropy associated with a large in-plane correlation length and a nearly complete turbostratic crystalline disorder. NanoG has thus a low number of ordered stacked layers and a high aspect ratio. The thickness of GNP samples reported in the literature, after the exfoliation treatments, is from several to dozens of nanometers and is thus of the same magnitude of nanoG. As mentioned in the "Introduction" section, these features of nanoG could favor the formation of filler networks and could also promote a remarkable mechanical reinforcement. It thus appears reasonable to adopt nanoG for the preparation of polymer nanocomposites. Moreover, the progressive delamination of the nanofiller induced by the mixing in the IR matrix could also be expected, as already demonstrated by some of the authors,[83] in the case of both pristine and organically modified clays.

COMPOSITES WITH NANOG AS THE ONLY FILLER

As shown in Table I, nanoG was added to the IR matrix in a wide range of concentrations, from 1 to 60 phr. Characterizations were performed on samples cross-linked with a typical sulphur-based system. Cross-linking curves are shown in Figure 2. The reversion of the cross-linking reaction was lower than 5%, and the values of both M_L and M_H increased with the nanoG content. As can be seen in Figure 2, the cross-linking reaction became faster as the nanoG content increased: t_{s1} and t_{90} values decreased from 13 to 4 min and from 19 to 10 min, respectively, passing from the neat IR matrix to the nanocomposite with 60 phr of nanoG. In the literature, the cross-linking reaction of NR was reported to be accelerated by a so-called functionalized graphite, obtained by thermal reduction of GO and containing about 9% of oxygen atoms.[54] The enhanced thermal conductivity of the

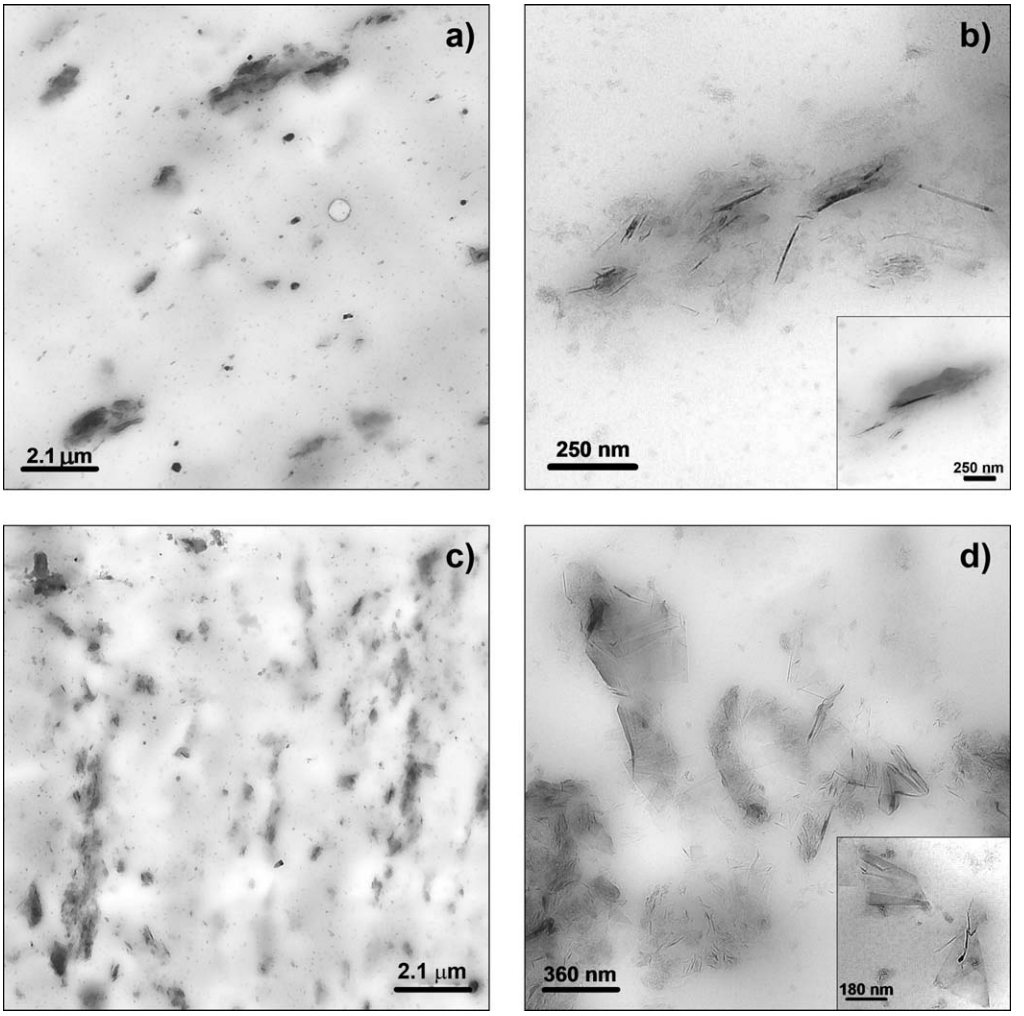

FIG. 3. — TEM micrographs at different magnifications of G-2 (a, b) and G-12 (c, d) cross-linked composites.

nanocomposite was proposed to be responsible for the faster curing reaction. Conversely, it is also reported in the literature that, with CNT as the carbon nanofiller, the curing reaction rate was lower than that of pure NR (Refs. 84 and 85) and the scorch time was longer.[86] The adsorption of curatives on CNT was hypothesized to cause higher curing activation energy and lower reactivity.[84,85] Analogously, in SBR as the polymer matrix, the curing time of the composites filled with CNTs was found to be longer than that of samples with CB.[87] The decrease of vulcanization time, scorch, and optimum cure time and the increase of the maximum torque was also found[88] by adding acid-treated and ball-milled CNT to NR. The effect of carbon nanofillers on vulcanization behavior seems to deserve further investigation. However, cross-linking data reported in this article allow us to conclude that polymer chains were properly cross-linked.

TEM analysis was performed to assess the distribution and degree of dispersion of nanoG into the IR matrix. Figures 3a and 3b show TEM micrographs of composites containing a low amount of nanoG, 2 phr. At low magnification (Figure 3a), G appears to be evenly distributed, with a fairly fine dispersion. Most agglomerates have submicrometric dimensions, some are about 5 μm large and

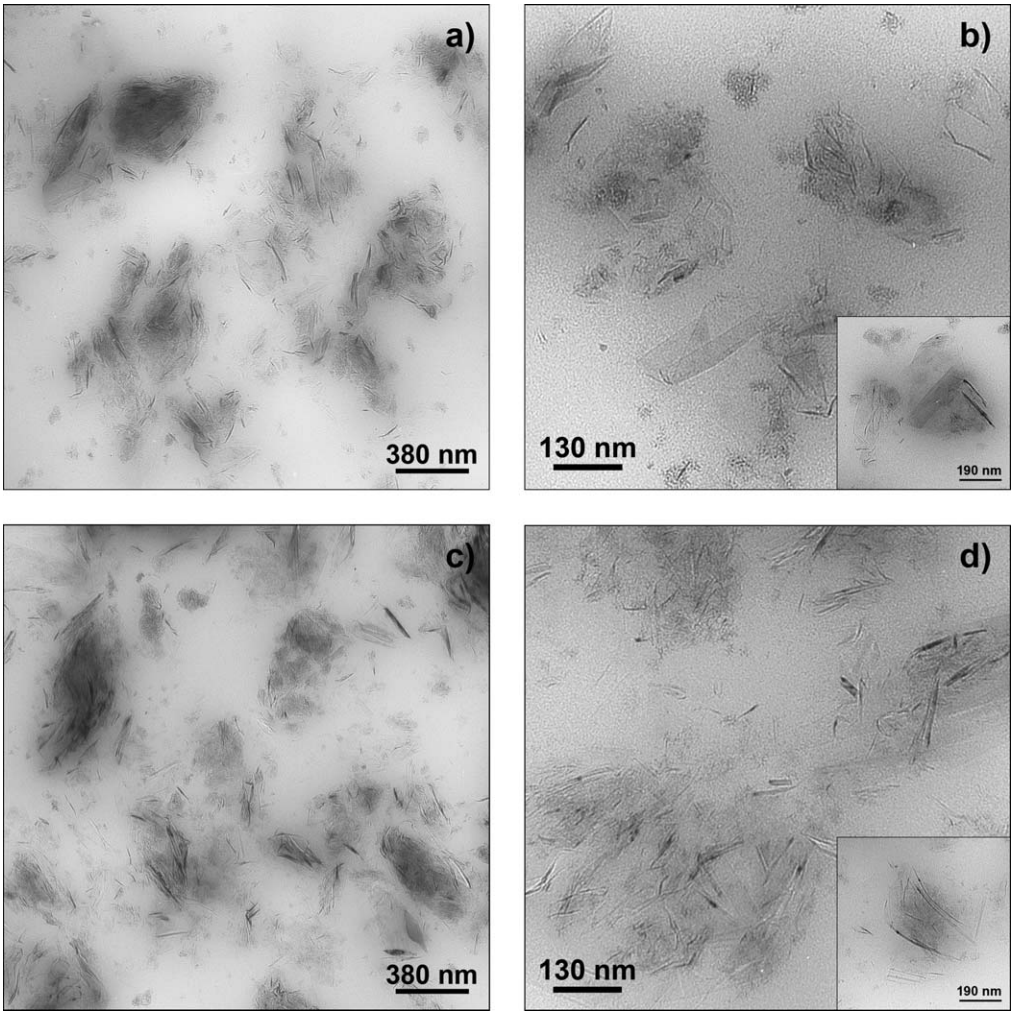

FIG. 4. — TEM micrographs of G-20 (a, b) and G-40 (c, d) cross-linked composites.

only a few are about 10 μm large. At higher magnification (Figure 3b), it is possible to observe a disordered placement of G layers inside the agglomerates and stacks of only a few G layers, as indicated by the stack thickness. It is thus possible to claim that nanocomposites were prepared from nanoG, being 100 nm the size threshold for having a nano-ingredient.[89] At this low content, nanoG particles do not form a continuous network in the IR matrix. Figures 3c and 3d show TEM micrographs of cross-linked composites containing a higher amount of nanoG: 12 phr. NanoG appears to be evenly distributed and highly delaminated (Figure 3c, low magnification). Moreover, it appears to form a network, although not continuous, made by nanoG agglomerates, few of which are about 7 μm large; some are about 3 μm large, and many are submicrometric sized. The agglomerates appear highly disordered. At higher magnification (Figure 3d and insert), few and single graphite layers appear located close to G agglomerates and, in a few cases, are dispersed in the IR matrix. Figure 4 shows TEM images of nanocomposites G-20 and G-40, containing 20 (Figures 4a and 4b) and 40 phr (Figures 4c and 4d) of nanoG, respectively. TEM images of both nanocomposites show, at low magnification, an even distribution of nanoG particles. A high level

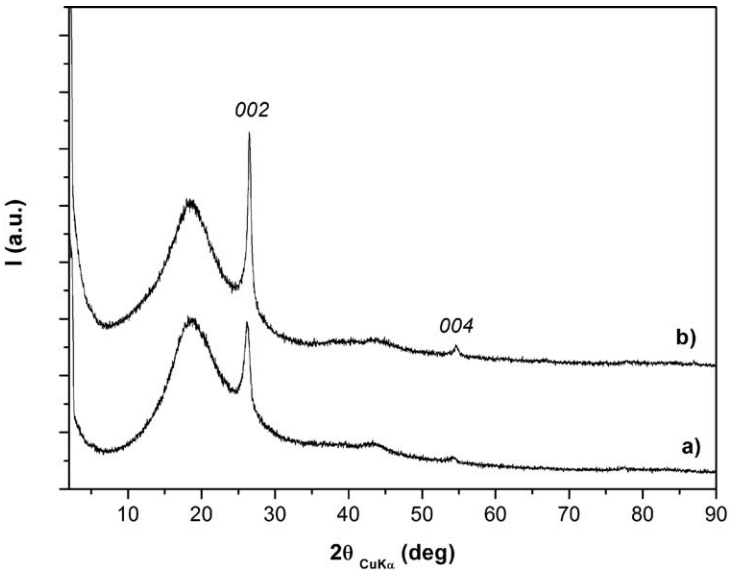

FIG. 5. — X-ray diffraction (CuKα) pattern in the 2θ range of 2 to 100° of G-12 composite.

of delamination was observed: agglomerates are not larger than 10 μm, and most are submicrometric sized and characterized by a disordered structure of the G layers. A very high amount of few and single graphite layers can be observed at higher magnifications, also in G-40, despite the high nanoG content. A continuous nanoG network within the IR matrix can be identified in micrographs of G-20 and is evident in TEM images of G-40.

XRD analysis was performed on the composites containing nanoG, to investigate the crystalline order of stacked layers in the polymer matrix. Figure 5 shows the XRD patterns of the sample with 12 phr as nanoG content as taken from the mixer, not cross-linked (Figure 5a), and cross-linked (Figure 5b).

Both patterns show a sharp peak at 26.2° as 2θ value, corresponding to the 002 reflection of nanoG. The Williamson-Hall plot could not be applied to determine the $D_{hk\ell}$ correlation lengths, because of the low intensity (absence) of reflections other than 002. $D_{hk\ell}$ were thus determined by applying the Scherrer equation (Eq. 1) to the 002 reflection. $D_{hk\ell}$ values of about 11 nm for the un-cross-linked sample and of 22 nm for the cross-linked sample were calculated. Taking into account that the d_{002} interlayer distance in a crystalline graphite is 0.339 nm, a number of about 32 and about 65 layers, stacked in an ordered manner, was estimated for the un-cross-linked and the cross-linked sample, respectively. Interestingly, the cross-linking step, which implies the application of a remarkable pressure (150 bar) on the rubber nanocomposites, promotes a higher degree of order in the graphite aggregates: a higher number of sheets become regularly stacked in crystalline domains. It could be proposed that the application of energy on a system makes the system move toward a minimum of energy, such as the nanoG crystallite. To the best of our knowledge, these findings are reported for the first time here.

Initial moduli values are collected in Table III. From these values and from the inspection of Figure 6, the E modulus is almost independent of the nanoG content up to 8 phr, increasing slightly between 12 and 20 phr and remarkably above 20 phr, in particular above 40 phr of nanoG.

In a second series of experiments, tensile tests were performed to assess the ultimate properties of the nanocomposites. Nominal stress–nominal strain curves are shown in Figure 7. As can be seen, the presence of nanoG leads to a worsening of ultimate properties of the nanocomposites,

TABLE III
VALUES OF E AND OF $G'(\gamma\ min)$ MODULI FOR CROSS-LINKED COMPOSITES CONTAINING NANOG AS THE ONLY FILLER[a]

Sample	G, phr	G, volume fraction	E, MPa	E standard deviation, MPa	$G'(\gamma\ min)$, MPa
G-0	0	0	1.31	0.045	0.43
G-1	1	0.0043	1.35	0.011	0.44
G-2	2	0.0086	1.41	0.026	0.44
G-4	4	0.0171	1.47	0.027	0.45
G-8	8	0.0337	1.59	0.022	0.47
G-12	12	0.0497	1.76	0.007	0.51
G-16	16	0.0652	1.95	0.13	0.56
G-20	20	0.0808	1.89	0.20	0.67
G-40	40	0.1495	4.83	0.51	1.24
G-60	60	0.2097	20.36	1.69	3.49

[a] Formulations are in Table I.

despite the good dispersion, high surface area, relatively high aspect ratio, and high shape anisotropy of the nanofiller. However, other factors can affect the ultimate properties of filled and cross-linked elastiomeric composites, for example, the filler–matrix adhesion, the cross-link density, and the strain crystallization behavior. The effect of nanoG on these factors is still unknown. The partial reaggregation of graphite sheets, shown by XRD analysis, could somehow favor the deterioration of ultimate properties. However, it is noteworthy that nanocomposites based on nanoG still show remarkable elongation at break, higher than 700% and 410%, even for nanoG content of 40 and 60 phr, respectively.

For filled polymer melts and elastomers, the dependence of the initial modulus on the filler concentration is expressed by the Guth-Gold-Smallwood equation[90–92]:

$$E/E_0 = 1 + 0.67f\phi + 1.62f^2\phi^2 \tag{2}$$

where E and E_0 are the initial modulus of the filled and unfilled matrix, respectively, ϕ is the filler volume fraction, the quadratic term accounts for the mutual disturbance caused by the spherical particles, and f is a shape factor that allows us to take into account the variation from the sphericity of

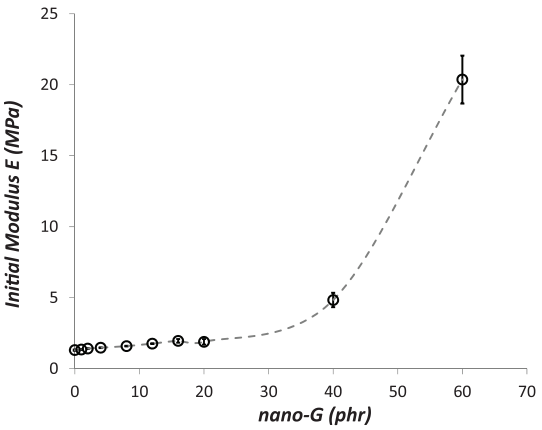

FIG. 6. — Initial modulus E, with standard deviations, for IR-based composites as a function of G content (see Table I for formulations and Table III for E values).

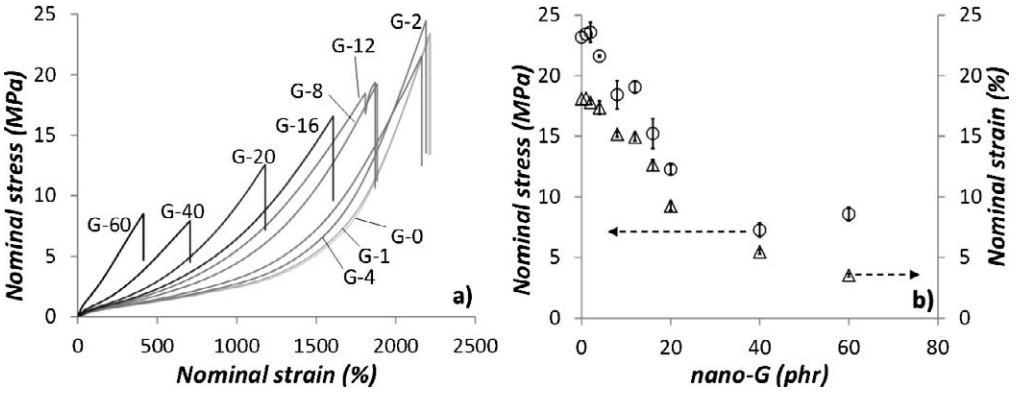

FIG. 7. — (a) Nominal stress–nominal strain curves obtained for cross-linked IR/nanoG composites of Table I; (b) nominal stress at break (open circles) and nominal strain at break (open triangles), with standard deviations, versus phr of nanoG.

particle aggregates. Equation 2 cannot be applied for ϕ values greater than a critical value, ϕ_p, defined as the filler volume fraction required to have filler percolation, a phenomenon that occurs when filler aggregates join together either by direct contact or via layer of polymer shell around them. Equation 2 was meant for spherical fillers, such as CB, but it has been applied to nanofillers, such as clays and CNT, calculating the *f* factor, considered as the aspect ratio of the nanofiller. In the case of clays, *f* factors equal to 26 and to 42 were found by melt blending an organoclay (with dimethyl ditalloyl ammonium as the compensating cation) with IR[8] and NR,[93] respectively. Interestingly, these *f* factors were in the range of clay aggregate dimensions estimated from TEM micrographs. In the case of CNT as nanofiller, the *f* values were as follows: from 15 to 20 when CNTs were melt mixed with a blend of a poly(1,3-butadiene) and poly(styrene-*co*-1,3-butadiene),[94] 22 when CNTs were melt blended with IR,[11] and 40 when SBR-based nanocomposites was prepared from solution blending.[95] These values were lower than those of pristine CNT and indicated that the mixing step drastically reduced the CNT length, as confirmed by the inspection of nanocomposites by TEM. In the present work, by applying Eq. 2 to initial modulus values of Table III, evaluated at strains lower than 0.15% (see the "Experimental" section, "Characterizations"), a good fitting was found up to $\Phi = 0.0155$ (14 phr of nanoG), with an *f* value of about 5.

The value of ϕ_p was determined by elaborating initial modulus data of Table III with a model proposed by Huber and Vilgis[96] for elastomers filled with nanostructured CB. According to this model, the excess of initial modulus $(E - E_0)/E_0$ has a linear dependence on the filler content below the percolation threshold and scales with a power law with exponent 4 for higher filler concentrations. The Huber-Vilgis model should be thus applied to composites containing spherical fillers. However, it was successfully adopted for composites containing nanofillers to a different extent far from sphericity, such as clay[8–10] and CNT.[11] A double logarithmic plot of the excess of *E* modulus as a function of CNT volume fraction was obtained from the data of Table III and is shown in Figure 8a. From the plot of Figure 8a, it is clear that experimental data can be linearly interpolated according to two different straight lines with slope 0.9 and 3.5, respectively. The point at which the two straight lines intersect each other gives the value of nanoG content required to achieve percolation. The nanoG percolation threshold is at a content of about 0.086 as volume fraction, which means at about 21.2 phr. In the literature, the percolation threshold for CB is shown to be in the range from 30 to 35 phr.[97,98]

Cross-linked samples from Table I were also characterized through dynamic-mechanical measurements. Strain sweep tests were carried out at 50 °C in the torsion mode, by applying a

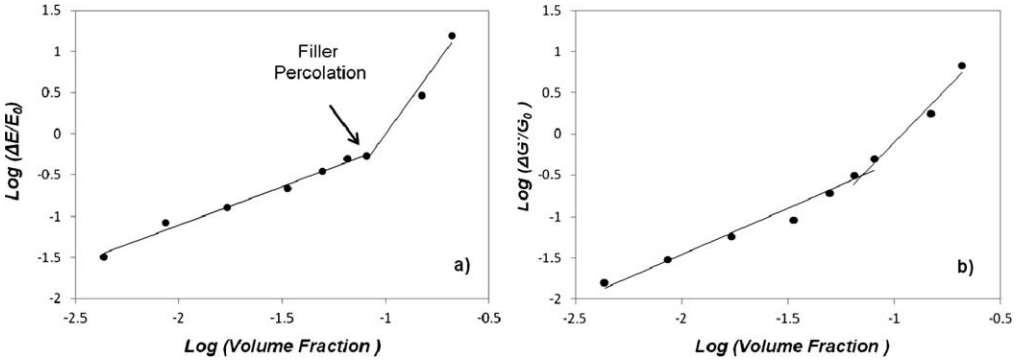

FIG. 8. — Huber–Vilgis double logarithmic plot: excess of modulus with respect to the unfilled matrix, $(E - E_0)/E_0$, as a function of the filler volume fraction for cross-linked composites containing nanoG (see Table I for formulations).

sinusoidal stress with a frequency of 1 Hz and a strain amplitude increasing from 0.1% to 25%. Dynamic shear storage G' and loss G'' moduli were determined as a function of the strain amplitude. The filler networking phenomenon was investigated by determining the dependence of the G' modulus at minimum deformation $G'(\gamma\ min)$ on the filler content and the dependence of G' and G'' moduli on nanoG content. Values of $G'(\gamma\ min)$ obtained for cross-linked samples of Table I are shown in Table III. The nanoG percolation threshold was determined from $G'(\gamma\ min)$ values by applying the Huber and Vilgis[96] model and calculating the excess of $G'(\gamma\ min)$ through the following equation (Eq. 3):

$$(G'(\gamma min) - G'_0(\gamma min))/G'_0(\gamma min) \tag{3}$$

where $G'_{0(}\gamma\ min)$ is the initial modulus of the composite without any filler. A double logarithmic plot was obtained, and it is shown in Figure 8b. The filler percolation threshold for nanoG was calculated to be at about 18 phr, a value not far from the one calculated from the E initial modulus values. This percolation threshold (at about 20 phr as nanoG concentration) appears to be higher than the one detected for OC (Ref. 8) and CNT,[11] at about 5.9 and 7.2 phr, respectively, but it is definitely lower than the one typical of nanostructured fillers, in particular of CB.

Figures 9a and 9b show the dependence on the strain amplitude of the storage G' and loss G'' moduli, respectively. It is known that the viscoelastic moduli of polymer melts and elastomers depend on the strain amplitude, besides frequency and temperature, in the presence of a filler

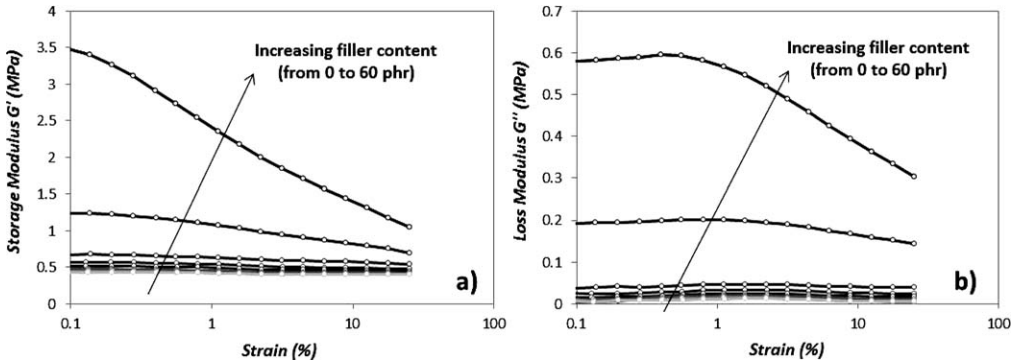

FIG. 9. — Behaviors of G' (a) and G'' (b) as a function of strain for composites containing different amounts of nanoG.

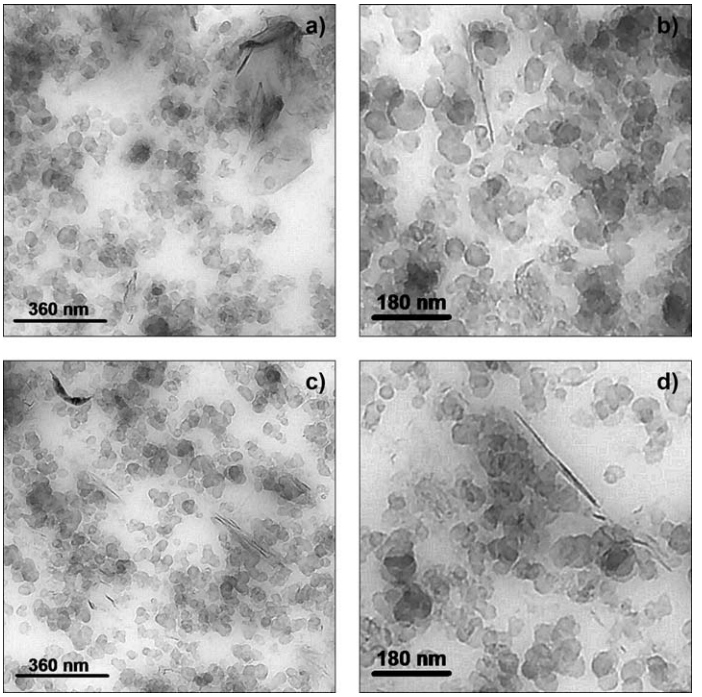

FIG. 10. — TEM micrographs of CB/G-2 (a, b) and CB/G-12 (c, d) cross-linked composites.

network. This nonlinear behavior is known as the Payne effect[99] and implies a reduction of G' as the strain increases and a variation of G'', which usually passes through a maximum. This phenomenon is due to the disruption of a secondary network formed when filler particles join together either by direct contact or via a layer of polymer shell around them. In Figure 9a, it is evident that remarkable values of $\Delta G' = (G'(\gamma\, min) - G'_{(25\%)})$ are obtained for the nanoG content of 40 and 60 phr, which are higher values than the nanoG percolation threshold. The maximum of the G'' curves reported in Figure 9b is in the range from 0.5% to 2% of strain amplitude, and it becomes more evident for nanoG contents above the percolation threshold.

COMPOSITES WITH NANOG AND CB

IR-based composites containing both CB and nanoG (Table II) were prepared to study the filler networking process promoted by a hybrid filler system formed by nanoG in the presence of a carbon allotrope. It was decided to adopt a CB concentration of 60 phr, suitable to form a CB network.[97,98] Composite morphology was investigated by means of TEM analysis, and some representative micrographs of composites containing 2 and 12 phr of nanoG are reported in Figure 10. TEM observations of composites containing 2 phr of nanoG indicate micrometric and submicrometric agglomerates of G within the IR matrix. As can be seen in Figures 10a and 10b, nanoG layers were found preferentially located close to CB agglomerates, thus revealing the high affinity of nanoG for the allotrope. An even nanoG distribution was detected also when the content of nanoG was 12 phr (Figure 10c,d). Submicrometric agglomerates and highly oriented aggregates made by few layers of nanoG were observed. A homogeneous hybrid CB–nanoG system was visible in TEM micrographs, whereas a continuous network made by the two fillers could not be identified.

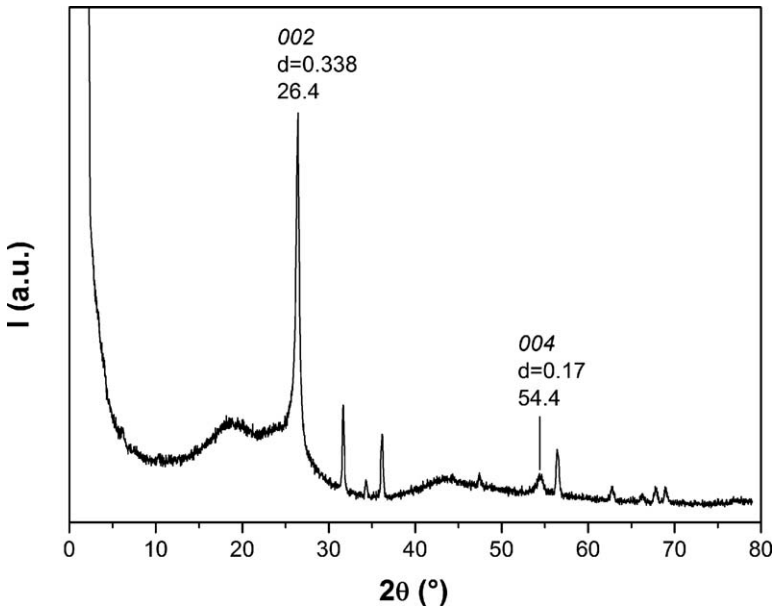

FIG. 11. — X-ray diffraction (CuKα) pattern in the 2θ range of 2 to 80° of the CB/G-5 cross-linked composite.

By using the concept and literature values of ZP, a comprehensive understanding of the microstructure of nanocomposites containing dual filler systems based on CB and a nanofiller was attempted in the literature.[79] At pH levels of rubber mixtures, ZP values are negative for nanofillers and are positive for CB types such as the one used in the present work. It was thus proposed that negatively charged nanoparticles (sepiolite and carbon nanofibers in Bhattacharya and Bhowmick[79]) can be attracted by a positively charged CB surface. The attraction between CB and clay was also documented.[100,101] Despite the fact that ZP measurements were not performed in the present work, these literature findings could justify the microstructure shown in TEM images of Figure 10 and support the formation of the hybrid CB–nanoG filler network.

The crystalline structure of nanoG in the composite containing CB as a further filler was investigated through XRD analysis. Figure 11 reports the XRD pattern of the cross-linked composite containing 12 phr of nanoG. In the pattern, a sharp peak at a 2θ value of 26.4° is evident, corresponding to the (002) reflection of G, which indicates the presence of highly ordered G stacks in nanoG. Moreover, the broad peak due to the crystallinity of CB can be noticed. It is known that the parallel graphitic layers are placed in a disordered way in CB, giving rise to the so-called turbostratic structure.[102]

As was done in the case of the pristine nanoG sample and in the case of the composite with nanoG as the only filler, the Scherrer equation (Eq. 1) was applied to the (002) reflection, determining a ($D_{\perp}$) value of about 30.2 nm and calculating a number of about 89 layers stacked in an ordered manner. It can be proposed that, passing from the pristine nanoG to cross-linked composites, with and without CB, the crystalline order in the direction perpendicular to the structural layers appears to increase. Also for these composites, with the hybrid filler system, the effect of the high pressure applied for the cross-linking step has to be taken into account.

Cross-linked composites of Table II were characterized by tensile measurements, similar to what was done for composites without CB. The initial elastic modulus was determined as the slope at the origin of the nominal stress–nominal strain curves, and its reproducibility was evaluated over three repetitions. Data of *E* modulus are shown in Table IV. It is evident, by taking into account the

TABLE IV
VALUES OF E AND OF $G'(\gamma\ min)$ FOR CROSS-LINKED COMPOSITES CONTAINING NANOG AND CB[a]

Sample	NanoG, phr	NanoG, volume fraction	E, MPa	E standard deviation, MPa	$G'(\gamma\ min)$, MPa
CB/G-0	0	0	8.30	0.94	3.00
CB/G-1	1	0.0038	8.10	0.62	3.13
CB/G-2	2	0.0075	10.07	0.91	3.25
CB/G-4	4	0.0149	7.88	0.46	3.43
CB/G-6	6	0.0222	9.69	0.65	3.60
CB/G-8	8	0.0293	9.83	0.82	3.91
CB/G-12	12	0.0434	14.9	1.5	4.54

[a] Formulations are in Table II.

fluctuating behavior of data, that the E modulus remains substantially unaltered up to about 6–8 phr of nanoG content, whereas an appreciable increase occurs for nanoG content equal to 12 phr.

In a second series of experiments, tensile tests were performed, achieving the elongation at break for all the samples. Figure 12 shows that nanocomposites containing nanoG are able to attain remarkable elongations at break, despite the presence of 60 phr of CB. The negative effect of nanoG on stress and strain at break can be observed, although it is less pronounced than that found for the compounds without CB. Analogous comments about this finding could be made, and, also for these nanocomposites based on the hybrid nanoG–CB filler system, the partial reaggregation of nanoG sheets, shown by XRD analysis, can be taken into consideration.

Composites containing 60 phr of either nanoG or CB can be directly compared: the inspection of Figure 7a and Figure 12a shows that the composite with CB is able to attain higher elongation at break, in line with what was commented above on the negative effect of nanoG on the ultimate properties. From the comparative analysis of data in Table III and in Table IV, similar G' values appear for composites with either 60 phr of nanoG or 60 phr of CB (3.0 and 3.5, respectively), whereas a large difference can be observed between the E values: 20.4 and 8.3 for composites with either nanoG or CB, respectively. This interesting finding could be due, at least in part, to the shape anisotropy of nanoG. However, it is also known that graphite is commonly used as a solid lubricant[103]: the layers glide under shear stress, due to weak van der Waals forces between them,

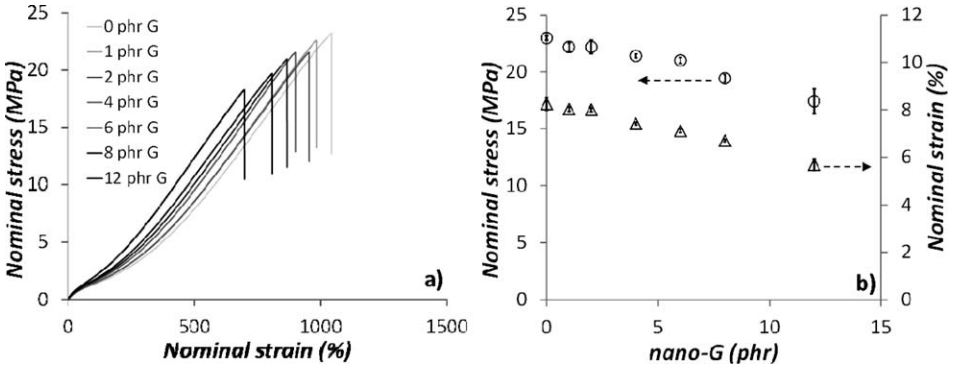

FIG. 12. — (a) Nominal stress-nominal strain curves obtained for cross-linked IR/CB/nanoG composites of Table II, containing 60 phr CB and different amounts of nanoG; (b) nominal stress at break (open circles) and nominal strain at break (open triangles), with standard deviations, versus phr of nanoG.

and low coefficient of friction (COF) and abrasion[104] are obtained. Further reduction of COF and wear has been reported for nanocomposites based on GNP in place of graphite,[59,60] and this result has been attributed to the formation of graphite lubricant film, without a direct contact with the friction surface. The remarkable increase of mechanical reinforcement due to nanoG seems thus to be lost when a shear stress is applied to the nanocomposite.

Cross-linked samples of Table II were characterized through dynamic-mechanical measurements, performing strain–sweep tests, applying the same procedure adopted for nanocomposites with nanoG as the only filler. Values of $G'(\gamma\ min)$ are collected in Table IV. Analogously to what observed for the E values, $G'(\gamma\ min)$ remains substantially unaltered up to about 6 to 8 phr as nanoG content and appreciably increases with 12 phr of nanofiller.

The E modulus and $G'(\gamma\ min)$ values of Table IV were elaborated, by applying the Huber-Vilgis model explained above, to investigate the presence of a discontinuity in the dependence of the excess of modulus on the nanofiller content. As mentioned above, the Huber-Vilgis model should be applied to composites containing one spherical filler. However, two regimes in the Huber-Vilgis plot were surprisingly observed for nanocomposites containing a hybrid filler system, based on CB and either OC (Ref. 8) or CNT,[11] suggesting the presence of a second percolation threshold.

NanoG/CB–based nanocomposites showed, analogously to what was reported for the samples with CB/OC (Ref. 8) and CB/CNT (Ref. 11) hybrid filler systems, a discontinuity in the dependence of the excess of modulus on nanoG content, as if nanoG and CB were able to establish a continuous hybrid filler network throughout the polymer matrix (although, as mentioned above, said continuous network was not easily identified in TEM micrographs). Elaborating E values and $G'(\gamma\ min)$ values, the mentioned discontinuity was determined to be at about 8 and about 6 phr, respectively. Analogously to CB/OC (Ref. 8) and CB/CNT (Ref. 11) hybrid filler systems, said discontinuity occurs at a nanofiller concentration lower than the one required to have the nanofiller percolation in the neat IR matrix. It could be commented that the presence of CB favors the dispersion of nanoG by enhancing the mixing stress. As a matter of fact, in TEM micrographs of Figure 10, nanoG agglomerates appear smaller than those present in TEM micrographs of Figure 4.

Strain sweep tests allowed us to investigate the dynamic-mechanical behavior at moderate deformations of the nanocomposites with the hybrid filler system by applying a strain amplitude up to 25%. The dependence of G' and G'' on the strain amplitude for composites of Table II is shown in Figures 13a and 13b, respectively. All of the composites show a nonlinear behavior also in the absence of nanoG, as should be expected taking into account that CB is at a concentration clearly above its percolation threshold. The addition of nanoG brings about an enhancement of the Payne effect, which appears appreciable for nanoG contents greater than 8 phr, a value mentioned above to bring about a shift from one regime to another for the dependence of the excess of modulus on nanoG content.

The pronounced enhancement of both $\Delta G'$ and G'' (in particular for 12 phr of nanoG) and the findings reported above for the E modulus (see the data in Table IV) suggest the investigation as to whether nanoG is able to develop a synergism with CB. In previous work on composites based CB/OC (Ref. 8) and CB/CNT (Ref. 11) hybrid filler systems, both nanofillers were found to develop a synergism with CB, which is said to occur when the value detected (for example) for the E modulus of the composite with the hybrid filler system is higher than the sum of the individual elements' contributions. Figure 14 shows that the values of the initial modulus, determined for composites containing both CB and nanoG (indicated by circles), are much higher than the values of $E_{IR/CB/nanoG}$ (dotted line) calculated through the following equation[105] (Eq. 4):

$$E_{IR/CB/nanoG} = E_{IR/CB} + E_{IR/nanoG} - E_{IR} \tag{4}$$

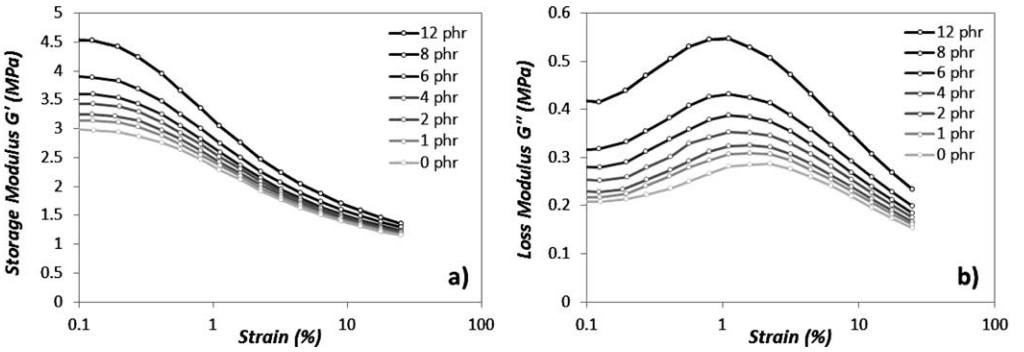

FIG. 13. — Dependence of G′ (a) and G″ (b) as a function of strain for composites containing CB and different amounts of nanoG.

where $E_{IR/CB}$ is the initial modulus of the composite containing 60 phr of CB (8.30 MPa; see Table IV), E_{IR} is the initial modulus of the IR matrix (1.31 MPa; see Table III), and $E_{IR/nanoG}$ is the initial modulus of the composite containing a given amount of nanoG in the neat IR matrix (see Table IV). For example, by adding 12 phr of nanoG to a neat IR matrix, the initial modulus E increases by 0.45 MPa, whereas the same amount of nanoG brings an increase of E of 6.58 MPa (see the data in Tables III and IV). On the basis of these findings, which demonstrate the interaction of CB and nanoG, and taking into consideration the information obtained from TEM (Figure 10), the pronounced enhancement of both $\Delta G'$ and G'' (Figure 13), and what was mentioned above on the discontinuity in the dependence of the excess of modulus on nanoG content, nanoG and CB can be considered to form a hybrid filler network, as already reported for CB/OC (Ref. 8) and CB/CNT (Ref. 11) systems.

CONCLUSIONS

A pristine nanoGraphite (nanoG), without any pretreatment to reduce the number of stacked layers, was found to promote filler networking in poly(1,4-*cis*-isoprene), neat or in the presence of CB, at a relatively low concentration. NanoG had a high surface area and a high shape anisotropy,

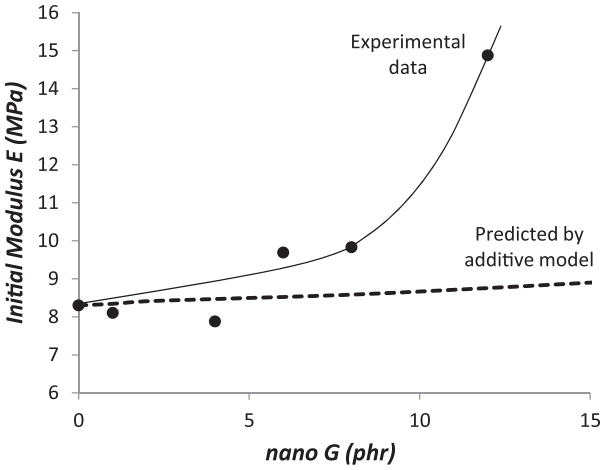

FIG. 14. — E initial modulus values for composites containing 60 phr of CB, as a function of the added nanoG (phr): experimental values (•), qualitative trend of experimental data (-), calculated values (- - -) (see text).

defined as the ratio between the out-of-plane correlation length ($D_{\perp}$) and the in-plane correlation length ($D_{\parallel}$). A quantitative determination of the percolation threshold in the neat polymer matrix was performed through tensile and dynamic-mechanical measurements, and a value of about 20 phr as nanoG content was found. In samples containing the hybrid filler system nanoG/CB (60 phr), a discontinuity was observed for the dependence of the excess of modulus on nanoG content, at about 6 phr as nanoG content, as if nanoG were able to establish a continuous network in the polymer matrix. These findings appear to be in line with what was already reported for other nanofillers such as OC and CNT, in the same matrices. TEM analysis revealed, in all of the samples, an even dispersion of nanoG and the presence of nanometric aggregates made also by few layers of graphene. Through XRD analysis, it was observed that the $D_{\perp}$ correlation length of nanoG aggregates remained substantially unchanged passing from pristine sample to the IR nanocomposite and increased upon performing the cross-linking reaction, thus suggesting the reorganization of nanoG in a liquid matrix, such as IR, upon applying a high pressure. Thus, nanoG behaves differently from clays, which experience a progressive exfoliation as a consequence of the mixing energy.

This work presents shape anisotropy as an important feature of a layered nanofiller such as a nanoGraphite. NanoG with a high shape anisotropy was successfully dispersed in an elastomer matrix as aggregates made by few layers, thus forming a continuous network at relatively low concentration without the need of any pretreatment and maintaining a long-range crystalline order within the layer. Further investigations need to be performed in order to assess the correlation between the nanofiller shape anisotropy and the nanocomposite properties. NanoG with high shape anisotropy appears to be the ideal candidate to achieve extensive exfoliation through the treatments reported in the prior art.[21–24]

ACKNOWLEDGEMENT

Professor Theonis Riccò (University of Brescia) is gratefully acknowledged for many useful discussions.

REFERENCES

[1]V. Mittal, *Advances in Polyolefin Nanocomposites*, CRC Press, Boca Raton, FL, 2011.

[2]M. Maiti, M. Bhattacharya, A. K. Bhowmick, RUBBER CHEM. TECHNOL. **81**, 384 (2008).

[3]J. B. Donnet and E. Custodero, "Reinforcement of Elastomers by Particulate Fillers," in *The Science and Technology of Rubber*, 3rd ed., J. E. Mark, B. Erman, F. R. Eirich, Eds., Elsevier Academic Press, 2005, p. 367.

[4]S. S. Ray and M. Okamoto, *Prog. Polym. Sci*. **28**, 1539 (2003).

[5]B. Chen, J. R. G. Evans, H. C. Greenwell, P. Boulet, P. V. Coveney, A. A. Bowden, and A. Whiting, *Chem. Soc. Rev*. **37**, 568 (2008).

[6]M. Galimberti, *Rubber Clay Nanocomposites: Science, Technology, Applications*, John Wiley and Sons, New York, 2011.

[7]L. Bokobza, *Polymer* **48**, 4907 (2007).

[8]M. Galimberti, M. Coombs, V. Cipolletti, P. Riccio, T. Ricco, S. Pandini, and L. Conzatti, *Appl. Clay Sci*. **65–66**, 57 (2012).

[9]G. Ramorino, F. Bignotti, S. Pandini, and T. Riccò, *Comp. Sci. Technol*. **69**, 1206 (2009).

[10]F. Schon and W. Gronski, *Kautsch. Gummi Kunstst*. **56**, 166 (2003).

[11]M. Galimberti, M. Coombs, P. Riccio, T. Riccò, S. Passera, S. Pandini, L. Conzatti, A. Ravasio, and I. Tritto, *Macromol. Mater. Eng*. **298**, 241 (2012).

[12]K. S. Novoselov, A. K. Geim, S. V. Morozov, D. Jiang, Y. Zhang, S. V. Dubonos, I. V. Grigorieva, and A. A. Firsov, *Science* **306**, 666 (2004).

[13]A. K. Geim and A. H. MacDonald, *Phys. Today* **60**, 35 (2007).

[14]E. T. Thostenson, C. Y. Li, and T. W. Chou, *Comp. Sci. Technol*. **65**, 491 (2005).

[15]S. Stankovich, D. A. Dikin, G. H. B. Dommett, K. M. Kohlhaas, E. J. Zimney, E. A. Stach, R. D. Piner, S. T. Nguyen, and R. S. Ruoff, *Nature* **442**, 282 (2006).

[16]S. Park and R. S. Ruoff, *Nat. Nanotech* **4**, 217 (2009).

[17]B. Z. Jang and A. Zhamu, *J. Mater. Sci*. **43**, 5092 (2008).

[18]T. Ramanathan, S. Stankovich, D. A. Dikin, H. Liu, H. Shen, S. T. Nguyen, and L. C. Brinson, *J. Polym. Sci. B, Polym. Phys*. **45**, 2097 (2007).

[19]B. Li and W.-H. Zhong, *J. Mater. Sci*. **46**, 5595 (2011).

[20]L. M. Viculis, J. J. Mack, O. M. Mayer, H. T. Hahn, and R. B. Kaner, *J. Mater. Chem*. **15***,* 974 (2005).

[21]A. V. Yakovlev, A. I. Finaenov, S. L. Zabud'kov, and E. V. Yakoleva, *J. Appl. Chem*. **79**, 1741 (2006).

[22]J. Li, H. Lin, W. Zhao, and G. Chen, *J. Appl. Polym. Sci*. **109**, 1377 (2008).

[23]H. Fan, L. Wang, K. Zhao, N. Li, Z. Shi, Z. Ge, and Z. Jin, *Biomacromol*. **11**, 2345 (2010).

[24]T. Ramanathan, S. Stankovich, D. A. Dikin, H. Liu, H. Shen, S. T. Nguyen, and L. C. Brinson, *J. Polym. Sci. B* **45**, 2097 (2007).

[25]F. Schedin, A. K. Geim, S. V. Morozov, E. W. Hill, P. Blake, M. I. Katsnelson, and K. S. Novoselov, *Nat. Mater*. **6**, 652 (2007).

[26]J. S. Bunch, A. M. van der Zande, S. S. Verbridge, I. W. Frank, D. M. Tanenbaum, J. M. Parpia, H. G. Craighead, and P. L. McEuen, *Science* **315***,* 490 (2007).

[27]X. Li and G. H. Chen, *Mater. Lett*. **63***,* 930 (2009).

[28]M. Toyoda, *Carbon* **46**, 1627 (2008).

[29]F. Vieira, I. Cisneros, N. G. Rosa, G. M. Trindade, and N. D. S. Mohallem, *Carbon* **44**, 2590 (2006).

[30]J. R. Potts, D. R. Dreyer, C. W. Bielawski, and R. S. Ruoff, *P*olymer **52**, 5 (2011).

[31]R. Sengupta, M. Bhattacharya, S. Bandyopadhyay, and A. K. Bhowmicka, *Progress in Polymer Science* **36**, 638 (2011).

[32]X. Jiang and L. T. Drzal, *Polym. Comp*. **31**, 1091 (2010).

[33]A. Delgado, F. Addiego, S. Ahzi, S. Patlazhan, V. Toniazzo, and D. Ruch, *IOP Conf. Ser. Mater. Sci. Eng*. **31**, 012009 (2012).

[34]F. Li, J. H. Zhu, S. Y. Wei, J. Ryu, L. Y. Sun, and Z. H. Guo, *Macromol. Chem. Phys*. **212**, 1951 (2011).

[35]K. Kalaitzidou, H. Fukushima, P. Askeland, and L. T. Drzal, *J. Mater. Sci*. **43**, 2895 (2008).

[36]D. Wang, X. Zhang, J.-W. Zha, J. Zhao, Z.-M. Dang, and G.-H. Hub, *Polymer* **54**, 1916 (2013).

[37]J. U. Roh, S. W. Mab, W. Lee, H. T. Hahn, and D. W. Lee, *Compos. Part B* **45**, 1548 (2013).

[38]Y. Han, Y. Wu, M. Shen, X. Huang, J. Zhu, and X. Zhang, *J. Mater. Sci*. **48**, 4214 (2013).

[39]G. Filippone, M. S. de Luna, D. Acierno, and P. Russo, *Polymer* **53**, 2699 (2012).

[40]A. Al-Jabareen, H. Al-Bustami, H. Harel, and G. Marom, *J. Appl. Polym. Sci*. **128**, 1534 (2013).

[41]L. Zhang, J. Q. Zhu, W. B. Zhou, J. Wang, and Y. Wang, *Energy* **39**, 294 (2012).

[42]M. Singhi and M. Fahim, *Polym. Comp*. **33**, 675 (2012).

[43]H. Quan, B.-Q. Zhang, Q. Zhao, R. K. K. Yuen, and R. K. Y. Li, *Composites Part A* **40**, 1506 (2009).

[44]M. D. Via, J. A. King, J. M. Keith, I. Miskioglu, M. J. Cieslinski, J. J. Anderson, and G. R. Bogucki, *J. Appl. Polym. Sci*. **124**, 2269 (2012).

[45]F. He, S. Lau, H. L. Chan, and J. Fan, *Adv. Mater*. **21**, 710 (2009).

[46]S. Kumar, L. L. Sun, S. Caceres, B. Li, W. Wood, A. Perugini, R. G. Maguire, and W. H. Zhong, *Nanotechnology* **21**, 105702 (2010).

[47]E. Narimissa, R. Gupta, M. Bhaskaran, and S. Sriramb, *Polym. Degrad. Stab*. **97**, 829 (2012).

[48]A. P. Yu, P. Ramesh, X. B. Sun, E. Bekyarova, M. E. Itkis, and R. C. Haddon, *Adv. Mater*. **20**, 4740 (2008).

[49]N. Yan, H. Xia, J. Wu, Y. Zhan, G. Fei, and C. Chen, *J. Appl. Polym. Sci*. **127**, 933 (2013).

[50]C. Li, C. Feng, Z. Peng, W. Gong, and L. Kong, *Polym. Comp*. **34**, 88 (2013).

[51]J. R. Potts, O. Shankar, S. Murali, L. Du, and R. S. Ruoff, *Comp. Sci. Technol*. **74**, 166 (2013).

[52]J. R. Potts, O. Shankar, L. R.Du, and S. Ruoff, *Macromolecules* **45**, 6045 (2012).

[53]A. Malas, C. K. Das, A. Das, and G. Heinrich, *Mater. Design* **39**, 410 (2012).

[54]M. M. del Hernaìndez, Mar Bernal, R. Verdejo, T. A. Ezquerra, and M. A. Loìpez-Manchado, *Comp. Sci. Technol*. **73**, 40 (2012).

[55]J. Yang, M. Tian, Q.-X. Jia, J.-H. Shi, L.-Q. Zhang, S.-H. Lim, Z.-Z. Yu, and Y.-W. Mai, *Acta Mater*. **55**, 6372 (2007).

[56]M. Bhattacharya, M. Maiti, and A. K. Bhowmick, *Polym. Eng. Sci*. **49**, 81 (2009).

[57]S.H. Song, H. K. Jeong, and Y. G. Kang, *J. Industrial Eng. Chem*. **16**, 1059 (2010).

[58]S. H. Song, H. K. Jeong, Y. G. Kang, and C. T. Cho, *Korean J. Chem. Eng*. **27**, 1296 (2010).

[59]L. L. Wang, L. Q. Zhang, and M. Tian, *Mater. Design* **39**, 450 (2012).

[60]L. Wang, L. Zhang, and M. Tian, *Wear* **276–277**, 85 (2012).

[61]J. Yang, M. Tian, Q.-X. Jia, L.-Q. Zhang, and X.-L. Li, *J. Appl. Polym. Sci*. **102**, 4007 (2006).

[62]F. R. Al-Solamya, A. A. Al-Ghamdib, and W. E. Mahmoud, *Polym. Adv. Technol*. **23**, 478, (2012).

[63]J. Yang, L.-Q. Zhang, J.-H. Shi, Y.-N. Quan, L.-L. Wang, and M. Tian, *J. Appl. Polym. Sci*. **116**, 2706 (2010).

[64]V. Sridhar, D. Xu, T. T. Pham, S. P. Mahapatra, and J. K. Kim, *Polym. Comp*. **30**, 334 (2009).

[65]Q. H. Mu and S. Y. Feng, *Thermochim. Acta* **462**, 70 (2007).

[66]M. Mauro, V. Cipolletti, M. Galimberti, P. Longo, and G. Guerra. *J. Phys. Chem. C* **116**, 24809 (2012).

[67]L. A. Wood and N. J. Bekkedall, *J. Appl. Phys*. **17**, 362 (1946).

[68]A. N. Gent, *Trans. Faraday Soc*. **50**, 521 (1954).

[69]P. J. Phillips and N. Vatansever, *Macromolecules* **20**, 2138 (1987).

[70]G. Allegra and M. Bruzzone, *Macromolecules* **16**, 1167 (1983).

[71]I. S. Choi and C. M. Roland, RUBBER CHEM. TECHNOL. **70**, 202 (1997).

[72]B. Huneau, RUBBER CHEM. TECHNOL. **84**, 425 (2011).

[73]N. S. Souza, A. D. Rodrigues, C. A. Cardoso, H. Pardo, R. Faccio, A. W. Mombru, J. C. Galzerani, O. F. de Lima, S. Sergeenkov, and F. M. Araujo-Moreira, *Phys. Lett. A* **376**, 544 (2012).

[74]M. Lotya, Y. Hernandez, P. J. King, R. J. Smith, V. Nicolosi, L. S. Karlsson, F. M. Blighe, S. De, Z. Wang, I. T. McGovern, G. S. Duesberg, and J. N. Coleman, *J. Am. Chem. Soc*. **131**, 3611 (2009).

[75]H. Zhu, C. Zhang, Y. Tang, J. Wang, B. Ren, and Y. Yin, *Carbon* **45**, 203 (2007).

[76]V. K. Paruchuri, A. V. Nguyen, and J. D. Miller, *Colloids* and Surfaces A *Physicochem. Eng. Aspects* **250**, 519 (2004).

[77]A. S. Dukhin and P. J. Goetz, *Ultrasound for Characterizing Colloids: Particle Sizing, Zeta Potential and Rheology, in Studies in Interface Science*, Vol. 15, D. Möbius and R. Miller, Eds., Elsevier, Amsterdam, 2002.

[78]V. N. Moraru, F. D. Ovcharenko, Z. M. Yaremko, and L. E. Moraru, *Colloid J. USSR* **42**, 738 (1980).

[79]M. Bhattacharya and A. K. Bhowmick, *J. Mater. Sci*. **45**, 6126 (2010).

[80]F. Brochard-Wyart and P. de Gennes, *Eur. Phys. J*. **E1**, 93 (2000).

[81]F. Flores, D. Graebling, A. Allal, and C. Guerret-Pi'ecourt, *J. Phys. D Appl. Phys*. **40**, 2911 (2007).

[82]H. P. Klug and L. E. Alexander, *X-Ray Diffraction Procedures: For Polycrystalline and Amorphous Materials,* Wiley, New York, 1959, Ch. 9.

[83]M. Galimberti, A. Lostritto, A. Spatola, and G. Guerra, *Chem Mater*. **19**, 2495 (2007).

[84]G. Sui, W. H. Zhong, X. P. Yang, Y. H. Yu, and S. H. Zhao, *Polym. Adv. Technol*. **19**, 1543 (2008).

[85]G. Sui, W. H. Zhong, X. P. Yang, Y. H. Yu, and S. H. Zhao, *Mater. Sci. Eng. A* **485**, 524 (2008).

[86]A. M. Shanmugharaj, J. H. Bae, K. Y. Lee, W. H. Noh, S. H. Lee, and S. H. Ryu, *Compos. Sci. Technol*. **67**, 1813 (2007).

[87]L. Lu, Y. Zhai, Y. Zhang, C. Ong, and S. Guo, *Appl. Surf. Sci*. **255**, 2162 (2008).

[88]G. Sui, W. H. Zhong, X. P. Yang, Y. H. Yu, S. H. Zhao, *Polym. Adv. Technol*. **19**, 1543 (2008).

[89]Scientific Committee on Emerging and Newly-Identified Health Risks, 21. http://ec.europa.eu/health/ph_risk/committees/04_scenihr/docs/scenihr_o_010.pdf. Accessed date June 22, 2007.

[90]E. Guth, *J. Appl. Phys*. **16**, 20 (1945).

[91]H. M. Smallwood, *J. Appl. Phys*. **15**, 758 (1944).

[92]E. Guth and O. Gold, *Phys. Rev*. **53**, 322 (1938).

[93]G. Ramorino, F. Bignotti, S. Pandini, and T. Riccò, *Comp. Sci. Technol*. **69**, 1206 (2009).

[94]A. Das, K. W. Stöckelhuber, R. Jurk, M. Grenzer, J. Fritzsche, H. Lorenz, M. Klüppel, and G. Heinrich, *Polymer* **49**, 5276 (2008).

[95]L. Bokobza, *Polymer* **48**, 4907 (2007).

[96]G. Huber and T. A. Vilgis, *Kaut. Gummi Kunstst*. **52**, 102 (1999).

[97]M. Klüppel and G. Heinrich, RUBBER CHEM. TECHNOL. **68**, 623 (1995).

[98]A. M. Y. Ellawindy, *Polym. Compos*. **24**, 1 (2003).

[99]A. R. Payne and R. E. Whittaker, RUBBER CHEM. TECHNOL. **44**, 440 (1971).

[100]Y. Konishi and M. Cakmak, *Polymer* **46**, 4811 (2005).

[101]J. F. Feller, S. Bruzaud, and Y. Grohens, *Mater. Lett*. **58**, 739 (2004).

[102]Z. Q. Li, C. J. Lu, Z. P. Xia, Y. Zhou, and Z. Luo, *Carbon* **45**, 1686 (2007).

[103]D. D. L. Chung, *J. Mater. Sci*. **37**, 1475 (2002).

[104]Y. Zhou, K. Hirao, Y. Yamauchi, and S. Kanzaki, *J. Am. Ceram. Soc*. **86**, 991 (2003).

[105]S. S. Sternstein, G. Ramorino, B. Jang, and A.-J. Zhu, RUBBER CHEM. TECHNOL. **78**, 258 (2005).

[*Received November 2012, Revised April 2013*]